Experimental

Tetraethoxysilane (TEOS), nitric acid, surfactant, and 2,5-diiodothiophene were mixed in tetrahydrofuran (THF) at room temperature for half an hour to form a precursor solution. The catalytic complex was formed by reacting palladium acetate, cuprous iodide, and triphenylphosphine (PPh_3) in THF. A typical synthesis utilizes a molar ratio of reactants of THF/HNO_3/TEOS/Brij-58/PPh_3/CuI/Pd$(OAc)_2$/2,5-diiodothiophene of 6.2:0.356:0.937:0.1:0.04:0.014:0.017:0.1, where Brij-58 is a non-ionic surfactant $CH_3(CH_2)_{15}(OCH_2CH_2)_{20}OH$. Films were prepared by either spin-coating the mixture of the catalytic complex and precursor solutions onto glass slides using a Specialty Coating Systems P-6000 spin-coater or allowing them to evaporate in a petri dish to form xerogels. The thin films were exposed to acetylene gas and triethylamine vapor at room temperature and 50 psi pressure for up to 3 days to polymerize the incorporated monomer. Pure conjugated PTE was obtained by washing with dilute HF to remove the silica and by ethanol extraction to remove the surfactant. The PTE was washed with ethanol to remove the unbound catalyst and partially dissolved in chloroform to achieve oligomeric PTE solutions that were subsequently coated on glass slides to form red oligomeric PTE films. The oligomeric PTE films were exposed to acetylene gas and the continuous reactions of acetylene with the active complex attached to the oligomers resulted in darkened films with increased UV-vis absorptions.

The nanocomposites were characterized by transmission electron microscope (TEM, JEOL 2010, operated at 200 kV), X-ray diffraction (XRD, Phillips Xpert X-ray diffractometer using Cu Kα radiation at $\lambda = 0.1542$ nm), UV-vis spectroscopy (Beckman DU460B UV-vis), Fourier transform infrared spectroscopy (FTIR, Thermo Nicolet Nexus 670 spectrophotometer with a Smart MIRacle horizontal attenuated total reflectance Ge crystal accessory), and by differential thermal analysis and thermogravimetric analysis (DTA/TGA, 2960 Simultaneous DTA–TGA by TA Instruments) operated at 10 °C min^{-1} from 30 to 1200 °C with argon sweep gas.

Received: January 28, 2003
Final version: April 10, 2003

[1] H. Eckert, M. Ward, *Chem. Mater.* **2001**, *13*, 3059.
[2] T.-Q. Nguyen, J. Wu, S. H. Tolbert, B. J. Schwartz, *Adv. Mater.* **2001**, *13*, 609.
[3] C.-G. Wu, T. Bein, *Science* **1994**, *266*, 1013.
[4] C.-G. Wu, T. Bein, *Chem. Mater.* **1994**, *6*, 1109.
[5] Y. Lu, Y. Yang, A. Sellinger, M. Lu, J. Huang, H. Fan, R. Haddad, G. Lopez, A. R. Burns, D. Y. Sasaki, J. Shelnutt, C. J. Brinker, *Nature* **2001**, *410*, 913.
[6] V. S.-Y. Lin, D. R. Radu, M.-K. Han, W. Deng, S. Kuroki, B. H. Shanks, M. Pruski, *J. Am. Chem. Soc.* **2002**, *124*, 9040.
[7] C. R. Martin, *Science* **1994**, *266*, 1961.
[8] D. J. Cardin, S. P. Constantine, A. Gilbert, A. K. Lay, M. Alvaro, M. S. Galletero, H. Garcia, F. Marquez, *J. Am. Chem. Soc.* **2001**, *123*, 3141.
[9] D. D. C. Bradley, *Adv. Mater.* **1992**, *4*, 756.
[10] W. J. Feast, J. Tsibouklis, K. L. Pouwer, L. Groenendaal, E. W. Meijer, *Polymer* **1996**, *37*, 5017.
[11] A. P. Davey, S. Elliott, O. O'Connor, W. Blau, *J. Chem. Soc., Chem. Commun.* **1995**, 1433.
[12] G. V. Tormos, P. N. Nugara, M. V. Lakshmikantham, M. P. Cava, *Synth. Met.* **1993**, *53*, 271.
[13] Y. S. Gal, B. Jung, S. K. Choi, *J. Appl. Polym. Sci.* **1991**, *42*, 1793.
[14] C.-J. Li, W. T. Slaven, V. T. John, S. Banerjee, *Chem. Commun* **1997**, *16*, 1569.
[15] J. Israelachvili, in *Intermolecular and Surface Forces*, 2nd ed., Academic Press Inc., San Diego, CA **1992**.
[16] A. Sellinger, P. M. Weiss, A. Nguyen, Y. Lu, R. A. Assink, C. J. Brinker, *Mater. Res. Soc. Symp. Proc.* **1998**, *519*, 95.
[17] A. Sellinger, P. M. Weiss, N. Anh, Y. Lu, R. A. Assink, W. Gong, C. J. Brinker, *Nature* **1998**, *394*, 256.
[18] C. J. Brinker, Y. Lu, A. Sellinger, H. Fan, *Adv. Mater.* **1999**, *11*, 579.
[19] R. H. Crabtree, in *The Organometallic Chemistry of the Transition Metals*, 3rd ed., Wiley-Interscience, New York **2001**.
[20] Y. Lu, G. Cao, R. P. Kale, S. Prabakar, G. P. Lopez, C. J. Brinker, *Chem. Mater.* **1999**, *11*, 1223.
[21] Q. Huo, D. I. Margolese, G. D. Stucky, *Chem. Mater.* **1996**, *8*, 1147.
[22] R. Giesa, *J. Macromol. Sci., Rev. Macromol. Chem. Phys.* **1996**, *C36*, 631.
[23] G. Shi, S. Jin, G. Xue, C. Li, *Science* **1995**, *267*, 994.
[24] W. T. I. V. Slaven, C.-J. Li, Y.-P. Chen, V. T. John, S. H. Rachakonda, *J. Macromol. Sci., Pure Appl. Chem.* **1999**, *A36*, 971.
[25] D. R. Rutherford, *Ph.D. Thesis*, Colorado State University, Fort Collins, CO **1989**, pp. 170.

Enhancement of Photocatalytic and Electrochromic Properties of Electrochemically Fabricated Mesoporous WO_3 Thin Films**

By *Sung-Hyeon Baeck*, *Kyoung-Shin Choi*, *Thomas F. Jaramillo*, *Galen D. Stucky*, and *Eric W. McFarland**

Tungsten oxide (WO_3) is an indirect bandgap semiconductor with interesting photoconductive behavior that has potential applications as a low cost material for solar energy devices.[1,2] Because of its distinct photochromic response and intercalation properties (H^+, Li^+, Na^+, and K^+),[3] it has also found use in electrochromic devices and chemical sensors. For the hydrogen cations, the electrochromic process of tungsten oxide has been explained on the basis of the double intercalation of a proton and an electron to form a colored tungsten bronze. WO_3 has been prepared by physical and chemical methods including sputtering and vacuum evaporation.[4] Electrochemical synthesis has been accomplished by stabilizing tungsten ions in sulfuric acid[5] or as a peroxo complex.[6,7] Because of the versatility of tungsten oxide in photo-electrochemical processes, the formation of high surface area, mesoporous tungsten oxide has also been of interest.[8–15] Synthesis of porous oxides has followed early work on catalytic functional materials such as MCM-41 using surfactants and block copolymers as templates.[16–21] Cheng et al.[9] reported enhanced electrochromic properties of sol–gel synthesized mesoporous tungsten oxide; however, the material did not exhibit long-range order of the pores. In general, synthesis of well-ordered tungsten or molybdenum oxides has been limited by the formation of Keggin ions and difficulties in promoting their three-dimensional condensation to give stable mesoporous structures.

We have recently described an electrochemical strategy for the production of thin nanostructured films by utilizing potential-controlled self-assembly of surfactant–inorganic aggregates at solid–liquid interfaces.[22] This approach manipulates surfactant–inorganic assemblies only in the thin interfacial region by electrochemically controlling surface interactions, which allows for the formation of nanostructured films from dilute surfactant solutions. After deposition, surfactants can

[*] Prof. E. W. McFarland, Dr. S.-H. Baeck, T. F. Jaramillo
Department of Chemical Engineering, University of California
Santa Barbara, CA 93106-5080 (USA)
E-mail: mcfar@engineering.ucsb.edu
Prof. G. D. Stucky
Department of Chemistry and Biochemistry, University of California
Santa Barbara, CA 93106-5080 (USA)
K.-S. Choi
Department of Chemistry, Purdue University
West Lafayette, IN 47907-2084 (USA)

[**] Major funding was provided by the Hydrogen Program of the Department of Energy (DOE, Grant # DER-FC36-01G011092). Partial funding and facilities were provided by the NSF-MRSEC funded Materials Research Laboratory (Award # DMR96-32716). Partial funding (GDS) was also supported by the National Science Foundation (NSF Grant # DMR02-33728).

 DOI: 10.1002/adma.200304669

ADVANCED MATERIALS

be easily removed from the pores by washing with a suitable alcohol. We have extended this methodology to generate electrochemically active mesoporous tungsten oxide films from the electrolyte containing a tungsten-peroxo complex as the inorganic precursor and sodium dodecyl sulfate (SDS) as the structure-directing agent. After deposition, the surfactant was extracted from the inorganic matrix by washing with ethanol. This was confirmed by X-ray photoelectron spectroscopy (XPS) and CHNO analysis (data not shown). We show that these films exhibit enhanced photocatalytic and electrochromic properties.

Deposition of tungsten oxide films using tungsten-peroxo complexes is usually carried out in aqueous solutions containing 30 vol.-% isopropanol, which improves the stability of peroxo complexes.[23,24] In the electrodeposition of mesoporous tungsten oxide, however, addition of isopropanol was found unnecessary because the 5 wt.-% SDS added as a structure-directing agent simultaneously acts as a stabilizer, preventing precipitation of peroxo complex for extended periods (> one month). The microporous surface features of the WO_3 films deposited in the presence of isopropanol and SDS are compared in the scanning electron micrographs (Figs. 1a,b, respectively). From these images, it is evident that addition of SDS significantly altered the morphologies of WO_3 deposits from spheres to needle-like shapes by affecting the crystal growth patterns at the micrometer-scale level during the deposition process.

Transmission electron microscopy (TEM) images revealed two distinctive types of mesostructures present in the films deposited with SDS, wormhole-like (Fig. 2a) and lamellar structures (Fig. 2b). The average pore size found in the wormhole-like structure is 25 Å and the lamellar structure is characterized by a wall thickness of 25 Å and an interlayer spacing of 15 Å. The dense and featureless image of the WO_3 particles from the control film deposited without SDS is also shown in Figure 2c for comparison, which confirms that the nanostructures are indeed fabricated through surfactant templating. It should be noted that the relative ratios of these two nanophases can be varied by changing the deposition potential, which directly affects the surface charge densities of the electrode and, therefore, the surface assembly patterns of the inorganic–surfactant aggregates. For example, while both

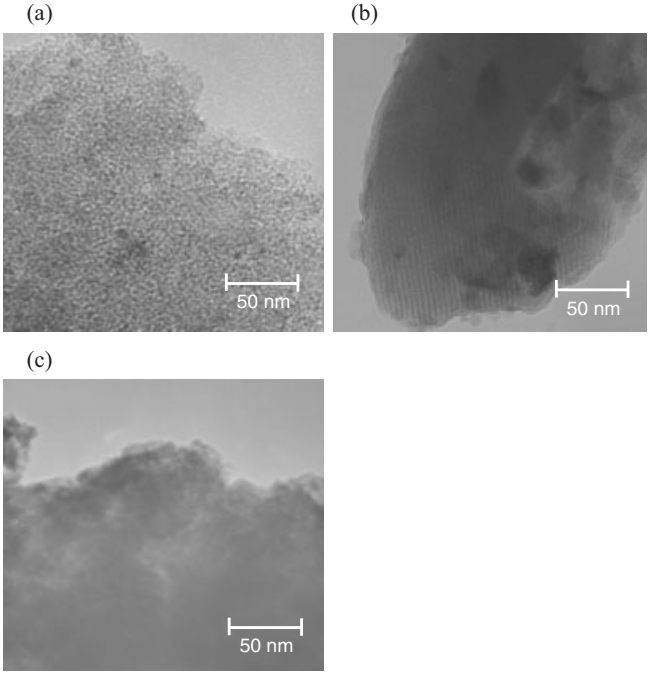

Fig. 2. TEM images of tungsten oxide films a) deposited at –0.2 V in the presence of SDS, yielding a wormhole-like structure, b) deposited at –0.5 V in the presence of SDS, resulting in a lamellar structure, and c) deposited at –0.5 V in the presence of isopropanol, which is dense and featureless.

structures are observed comparably in the films deposited at –0.2 V vs. Ag/AgCl reference electrode, the lamellar structure is predominant in films deposited at –0.5 V. This observation can be quantitatively confirmed by comparing the intensity of the diffraction peaks of the ordered lamellar structure in each sample, Figure 3.

Figures 3a,b show small angle X-ray diffraction patterns for the films deposited at –0.5 V and –0.2 V, respectively, with the same thickness (800 nm). Well-defined peaks appeared at 38.8 Å, 19.5 Å, and 12.7 Å and are indexed as 100, 200, and 300 reflections of the ordered lamellar phase with a repeat distance of 38.8 Å. This was also confirmed by two-dimensional grazing-incident small-angle X-ray scattering (2D-gi-SAXS) pattern of the WO_3 film. It is evident from these XRD patterns that the film deposited at –0.5 V possesses larger domains with an ordered lamellar structure resulting in much more intense diffraction peaks than those generated by the film deposited at –0.2 V. The wormhole-like structure present in these films does not generate any diffraction peak due to the lack of long-range order. The small-angle XRD patterns of the film deposited at –0.5 V and subsequently calcined at 450 °C is also shown in Figure 3c. The mesostructure is still present after 4 h of heat treatment, indicating considerable robustness of the electrochemically built layered structure. However, the decreased peak intensity in the XRD pat-

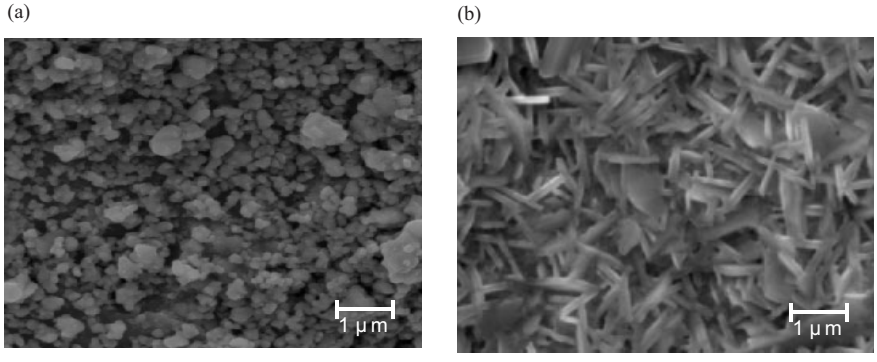

Fig. 1. Scanning electron micrographs (15 kV) of tungsten oxide films synthesized with a) isopropanol and b) sodium dodecyl sulfate (SDS).

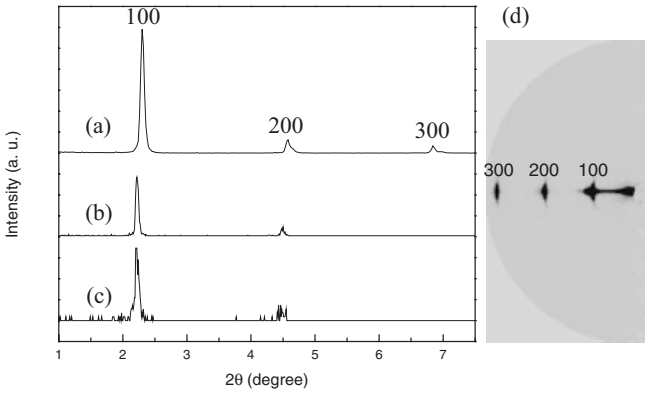

Fig. 3. Small angle X-ray patterns of mesoporous tungsten oxide films; a) as-synthesized at –0.5 V, b) as-synthesized at –0.2 V, c) after calcination of the film deposited at –0.5 V at 450 °C for 4 h, and d) 2D-giSAXS pattern of (a). All films were deposited on ITO substrates.

tern compared to that of as-synthesized films implies a gradual collapse of lamellar structures upon heating.

We investigated the photocatalytic activity and electrochromic properties of lamellar phase mesoporous tungsten oxide films. Throughout this work, we have normalized all current data to the geometric area of the electrode and to the weight of the tungsten oxide within that area (because of differences in morphology and density among samples), resulting in units of mA cm^{-2} mg^{-1} or μA cm^{-2} mg^{-1}. The measurement of photocurrent from a photoanodic film in an electrochemical cell is an indirect indicator of photocatalytic activity. We measured photocurrent at zero bias for the control film (deposited with isopropanol) and the lamellar phase mesostructured film (deposited with SDS) on indium tin oxide (ITO) substrates.

Illumination was provided by a chopped Xe light source (25 mW cm^{-2}) and the electrolyte consisted of 0.1 M sodium acetate, Figure 4. Prior to measurement of photocurrent, samples were calcined at 450 °C for 4 h to form the monoclinic

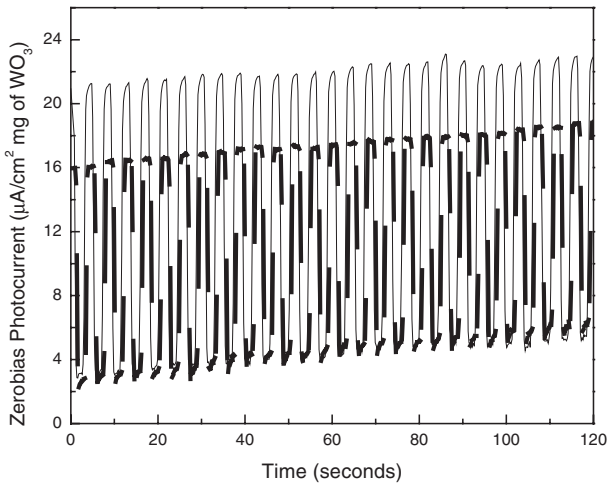

Fig. 4. Zero bias photocurrent of a lamellar phase mesoporous tungsten oxide film deposited in the presence of SDS (thin solid line) and the control film deposited in the presence of isopropanol (thick dashed line). Current direction indicates n-type semiconductor behavior. Illumination was provided by a 150 W Xe lamp.

structure of tungsten oxide and to decrease defect density.[6] The photo response of the lamellar phase mesoporous tungsten oxide film was 26.5 % higher than that of the control film, consistent with an increased surface area and the different surface morphologies, as shown in Figure 1. The values of zero bias photocurrent for the films prepared with surfactant and with isopropanol are 16.7 and 13.2 μA cm^{-2} mg^{-1} WO_3, respectively.

After washing with ethanol to remove surfactants, as-synthesized samples were investigated for hydrogen intercalation. Whereas calcination is required to achieve photocatalytic activity,[6] intercalation efficiency of tungsten oxide decreases with calcinations temperature.[3] Figures 5a,b exhibit the cyclic voltammogram measured in 0.5 M H_2SO_4 of the lamellar phase mesoporous tungsten oxide film deposited with SDS and the nonporous tungsten oxide film deposited with isopropanol. When the tungsten oxide films were cathodically polarized in H_2SO_4, the color of the film turned to blue, which intensified with increasing cathodic potential. When the blue films were anodically polarized, they were bleached. The integrated cathodic current density equates to the amount of hydrogen intercalated to form a tungsten bronze. When compared with the cathodic current of tungsten oxide deposited with isopropanol, the lamellar phase mesoporous tungsten oxide film clearly showed higher current density. At –0.5 V, the intercalation current for the lamellar phase mesoporous tungsten oxide was 1 mA cm^{-2} mg^{-1} WO_3 (1.8 mA cm^{-2}), compared to only 0.5 mA cm^{-2} mg^{-1} WO_3 (1.1 mA cm^{-2}) for the control material. These results indicate that to achieve the same coloring current, a lower potential can be used for lamellar phase mesoporous tungsten oxide films, which translates to greater efficiency. The improved hydrogen intercalation of lamellar tungsten oxide film can be attributed to its larger surface area, which delivers greater interfacial proton transfer.

Interestingly, double anodic current peaks were observed with lamellar phase mesoporous tungsten oxide during the bleaching process, which indicates that different electrochemical processes dominate in certain voltage ranges. The development of multiple peaks during de-intercalation of hydrogen was reported previously, and it was concluded that multiple peaks were caused by different types of hydrogen injection sites, such as shallow trap sites and deep trap sites.[9] To directly compare de-intercalation efficiencies, the two films were subjected to potential step chronoamperometry. Each electrode was first biased at –0.5 V vs. a Ag/AgCl reference electrode for 2 min to allow for cation intercalation. The polarity was then immediately switched to +0.5 V to initiate de-intercalation, and the current recorded, Figure 5c. The control (non-porous) film shows a rapid rise in current coincident with the voltage step. The current decays slowly relatively to the lamellar phase mesoporous film, indicating that this material performs slower with respect to cation de-intercalation. The lamellar phase mesoporous tungsten oxide, however, distinguishes itself from the control material in two ways. First, its initial jump in current is nearly three times that of the control film, indicating a more facile de-intercalation

ADVANCED MATERIALS

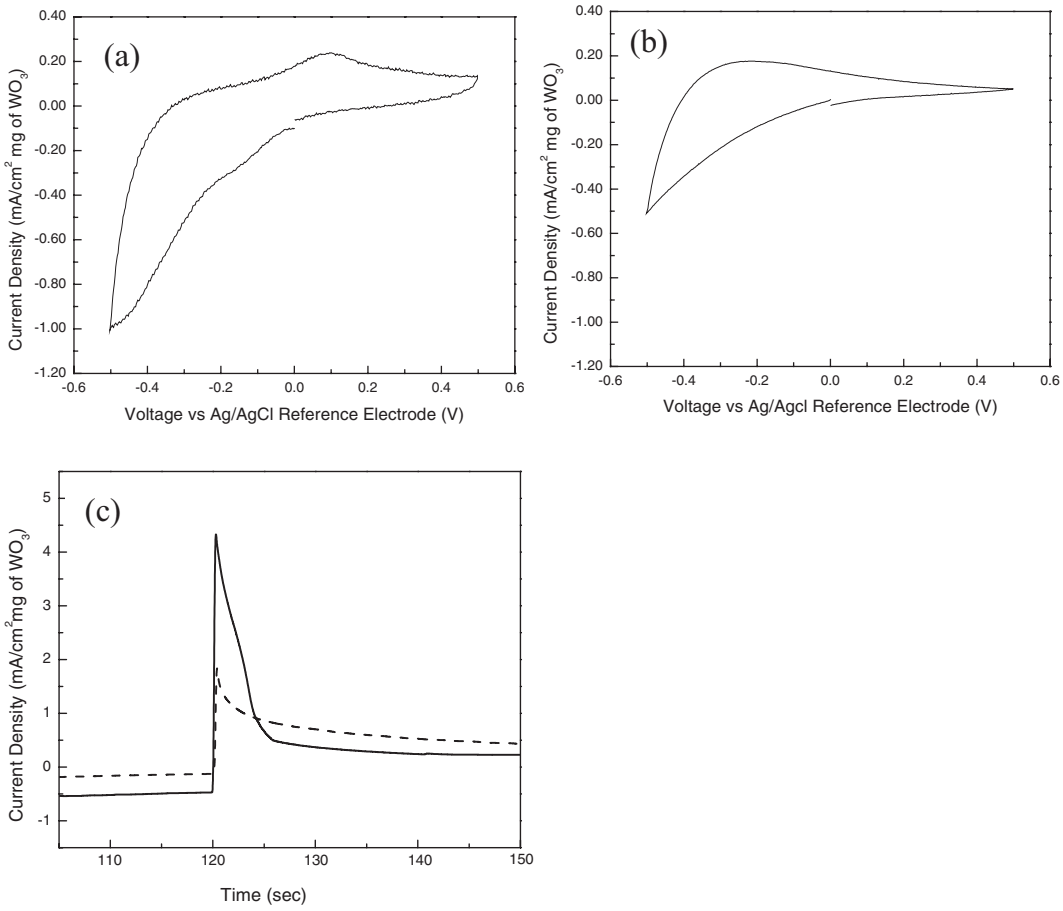

Fig. 5. Cyclic voltammogram for hydrogen intercalation/de-intercalation of a) the lamellar phase mesoporous tungsten oxide film deposited in the presence of SDS and b) the control film deposited in the presence of isopropanol. The scan rate was 100 mV s^{-1}. c) Chronoamperometry with voltage step from –0.5 V to +0.5 V (solid line: lamellar phase mesoporous tungsten oxide, dashed line: control film).

process at the start. Secondly, this current drops much more sharply than that of the control film; the majority of the cations that had been intercalated have been expunged within the first 5 s. Thus, not only does the lamellar phase mesoporous tungsten oxide intercalate more cations efficiently than the control material (as evidenced by Figs. 5a,b), but it is also more effective at de-intercalation, as shown in Figure 5c.

In summary, mesoporous tungsten oxide films with lamellar structure were successfully synthesized by electrodeposition using SDS as a templating agent. Compared to nonporous tungsten oxide prepared with isopropanol, lamellar phase mesoporous tungsten oxide showed higher photocatalytic activity and greater current density for hydrogen intercalation. Functional improvements are most probably due to the larger surface area of mesoporous tungsten oxide and facilitated charge transport.

Experimental

Electrolytes were prepared by dissolving 1.8 g of tungsten powder in 60 ml of 30 % hydrogen peroxide. After decomposing the excess hydrogen peroxide with platinum black, the solution was diluted to 50 mM with a 50:50 water and isopropanol mixture or sodium dodecyl sulfate solution. ITO-coated glass was used as cathodic substrate after cleaning with aqueous detergent, acetone, and isopropanol. A cylindrical Pt mesh was used as a counter electrode and the reference electrode was Ag/AgCl electrode in 4 M KCl saturated with AgCl. Electrodeposition was carried out potentiostatically at $-0.2 \leq V \leq -0.5$ against the reference electrode at room temperature without stirring. The resulting films were thoroughly washed with deionized water and ethanol for the removal of surfactant and dried in air. Following synthesis, representative films underwent more detailed quantitative analysis. Scanning electron microscopy (FEI, XL-30) was performed to give surface morphology and particle size, and X-ray diffraction (Scintag, X2) was used to examine crystalline structure. Photoelectrochemical screening of the samples for the measurement of zero bias photocurrent was performed with an electrochemical cell described in detail elsewhere [6]. Current data obtained while the surface is illuminated with a chopped light source (Oriel, Xe 150 W). Due to losses through the optical fiber, the light intensity incident on the sample was approximately 25 mW cm^{-2}. For measurement of hydrogen intercalation, Pt was used as a counter electrode and Ag/AgCl as a reference electrode in 0.5 M H_2SO_4 with the scan rate of 100 mV s^{-1}.

Received: November 21, 2002
Final version: April 24, 2003

[1] D. Le Bellac, A. Azens, C. G. Granqvist, *Appl. Phys. Lett.* **1995**, *66*, 1715.
[2] C. G. Granqvist, *Sol. Energy Mater. Sol. Cells* **2000**, *60*, 201.
[3] *Handbook of Inorganic Electrochromic Materials* (Ed: C. G. Granqvist), Elsevier, Amsterdam **1995**.
[4] J. L. Solis, A. Hoel, V. Lantto, C. G. Granqvist, *J. Appl. Phys.* **2001**, *89*, 2727.
[5] L. Su, L. Zhang, J. Fang, M. Xu, Z. Lu, *Sol. Energy Mater. Sol. Cells* **1999**, *58*, 133.

[6] S. H. Baeck, T. F. Jaramillo, C. Brändli, E. W. McFarland, *J. Comb. Chem.* **2002**, *4*, 563.
[7] S. H. Baeck, T. F. Jaramillo, G. D. Stucky, E. W. McFarland, *Nano Lett.* **2002**, *2*, 831.
[8] P. Yang, D. Zhao, D. I. Margolese, B. F. Chmelka, G. D. Stucky, *Nature* **1998**, *396*, 152.
[9] W. Cheng, E. Baudrin, B. Dunn, J. I. Zink, *J. Mater. Chem.* **2001**, *11*, 92.
[10] Q. S. Huo, D. I. Margolese, U. Cielsla, D. G. Demuth, P. Y. Feng, T. E. Gier, P. Sieger, A. Firouzi, B. F. Chmelka, F. Schüth, G. D. Stucky, *Chem. Mater.* **1994**, *6*, 1176.
[11] K. J. Balkus, Jr., M. E. Kinsel, *US Patent 6 120 891*, **1999**.
[12] C. L. Bowes, A. Malek, G. A. Ozin, *Chem. Vap. Deposition* **1996**, *2*, 97.
[13] U. Mueller, S. Bayer, G. Oetter, E. Gehrer, U. Ciesla, F. Schueth, A. Monnier, K. Unger, G. Stucky, *Eur. Patent 0 670 286*, **1995**.
[14] P. Yang, T. Deng, G. M. Whitesides, G. Stucky, D. Zhao, B. Chmelka, D. Pine, P. Feng, *US Patent* 6 541 539, **2003**.
[15] A. Stein, M. Fendorf, T. P. Jarvie, K. T. Mueller, A. J. Benesi, T. E. Mallouk, *Chem. Mater.* **1995**, *7*, 304.
[16] D. M. Antonelli, J. Y. Ying, *Chem. Mater.* **1996**, *8*, 874.
[17] P. Liu, S.-H. Lee, C. E. Tracy, Y. Yan, J. A. Turnar, *Adv. Mater.* **2002**, *14*, 27.
[18] H. Hujii, M. Ohtaki, K. Eguchi, *J. Am. Chem. Soc.* **1998**, *120*, 6832.
[19] Y. Sakamoto, M. Kaneda, O. Terasaki, D. Y. Zhao, J. M. Kim, G. Stucky, H. J. Shin, R. Ryoo, *Nature* **2000**, *408*, 449.
[20] U. Ciesla, M. Froba, G. Stucky, F. Schuth, *Chem. Mater.* **1999**, *11*, 227.
[21] D. T. On, *Langmuir* **1999**, *15*, 8561.
[22] K.-S Choi, H. C. Lichtenegger, E. W. McFarland, G. D. Stucky, *J. Am. Chem. Soc.* **2002**, *124*, 12 402.
[23] P. K. Shen, A. C. C. Tseung, *J. Mater. Chem.* **1992**, *2*, 1141.
[24] E. A. Meulenkamp, *J. Elecrochem. Soc.* **1997**, *144*, 1664.

Room-Temperature Synthesis of Aragonite Crystals at an Expanding Liquid–Liquid Interface in a Radial Hele–Shaw Cell**

By *Debabrata Rautaray*, *Arun Banpurkar*, *Sudhakar R. Sainkar*, *Abhay V. Limaye*, *Neela R. Pavaskar*, *Satish B. Ogale*, and *Murali Sastry**

Control over the crystallography and morphology of minerals is an important goal in the area of crystal engineering. Synthesis of advanced inorganic materials with control over crystallographic structure, size, and morphology is often driven by commercial requirements in areas as diverse as electronics, pigments, cosmetics, ceramics, and medical industries.[1,2] Insofar as ceramic engineering is concerned, much of the research has centered on the use of biomimetic templates such as Langmuir monolayers at the air–water[3a–d] and liquid–liquid interface,[3e] self-assembled monolayers (SAMs),[4] lipid-bilayer stacks,[5] and functionalized polymer surfaces[6] to achieve such control. Suitably designed additives in solution have also been used with success in controlling the morphology and structure of ceramic crystals.[5b,7] Attempts have also been made to synthesize oxides such as zinc oxide,[8a] gallium oxide,[8b] and ceramics such as $BaCrO_4$[8c] and $BaSO_4$[9] in microemulsions where interactions between surfactant molecules coating the crystallites were implicated in the assembly process.[8c,9]

Calcium carbonate is a relatively complex mineral system due to the existence of three stable polymorphs: calcite, aragonite, and vaterite.[10] Calcium carbonate crystallization has been achieved under Langmuir monolayers,[11] within lipid-bilayer stacks,[5c] using polymers,[6] bicontinuous emulsions,[12a] using mixed solutions of surfactants and block copolymers,[12b] on functionalized gold nanoparticles[13a] and monolayer films of gold nanoparticles,[13b] as well as on free nanoparticles in solution.[13c] The $CaCO_3$ polymorph aragonite is known to have a very high mechanical strength and is metastable under ambient conditions.[3c] A classical example is that of nacre in which growth of plate-like aragonite crystals occurs within a complex organic matrix.[3c] In comparison, the laboratory synthesis of aragonite at room temperature has been very difficult to achieve without the use of soluble additives such as small organic molecules or Mg^{2+} ions[13a,14a–c] but has been achieved at slightly elevated temperatures.[4a,14c,d] The exceptions are reports of Litvin et al.[3c] and Heywood and Mann[15] where the formation of aragonite crystals at the air–water interface using compressed monolayers of 5-hexadecyloxyisophthalic acid[3c] and under monolayers of eicosanoic acid and *n*-eicosyl sulfate[15] has been demonstrated. Another important report on the room-temperature synthesis of aragonite crystals is that of Falini et al. who have shown that this polymorph may be grown in vitro by treatment of layers of aragonite-associated glycoproteins assembled on β-chitin-silk fibroin substrates.[16] The aragonite-associated glycoproteins were extracted from aragonitic shell layers of some mollusks.[16] Küther et al. have also observed growth of aragonite needles, albeit at a slightly elevated temperature (45 °C) on SAMs of an anthracene-terminated thiol that was observed to assemble in a rectangular lattice.[4a]

In the biomimetic templated crystal growth methods studied thus far,[3–15] the charged interface at which crystal synthesis is carried out is static. To the best of our knowledge, there are no reports investigating the role of an *expanding charged interface* on mineral growth. We attempt to address this lacuna and demonstrate herein the synthesis of $CaCO_3$ crystals at the steadily expanding interface between two liquids (an aqueous solution of $CaCl_2$ and Na_2CO_3 and a chloroform solution containing aerosol OT) in a radial Hele–Shaw apparatus (Fig. 1a).[17a] The anionic surfactant sodium bis-2-ethylhexyl-sulfosuccinate (aerosol OT, AOT) is a twin tailed surfactant most commonly used to make reverse micelles and has been used with success in the synthesis of nanoparticles of barium chromate,[8c] barium sulfate,[9] calcium sulfate,[18a] barium carbonate,[18b] and silica.[18c] In the Hele–Shaw cell, we observe the room-temperature growth of large quantities of extremely fine aragonite needles. By simple variation of the

[*] Dr. M. Sastry, D. Rautaray, Dr. S. R. Sainkar, Dr. N. R. Pavaskar
Materials Chemistry Division, National Chemical Laboratory
Pune 411008 (India)
E-mail: sastry@ems.ncl.res.in
Dr. A. Banpurkar, Dr. A. V. Limaye
Centre for Advanced Studies in Materials Science
Department of Physics, University of Pune
Pune 411007 (India)
Dr. S. B. Ogale
Department of Physics, University of Maryland
College Park, MD 20742 (USA)

[**] DR thanks the Department of Science and Technology (DST), Govt. of India for financial support.

 DOI: 10.1002/adma.200304535